

Article

Spatial Distributions and Sources of Inorganic Chlorine in PM_{2.5} across China in Winter

Li Luo ^{1,2} , Yong-Yun Zhang ², Hua-Yun Xiao ^{1,*}, Hong-Wei Xiao ^{1,*}, Neng-Jian Zheng ¹, Zhong-Yi Zhang ¹, Ya-Jun Xie ¹ and Cheng Liu ¹

¹ Jiangxi Province Key Laboratory of the Causes and Control of Atmospheric Pollution, East China University of Technology, Nanchang 330013, China

² School of Water Resources and Environmental Engineering, East China University of Technology, Nanchang 330013, China

* Correspondence: xiaohuayun@ecit.cn (H.-Y.X.); xiaohw@ecit.cn (H.-W.X)

Received: 7 August 2019; Accepted: 27 August 2019; Published: 29 August 2019



Abstract: Chlorine is an important atmospheric photochemical oxidant, but few studies have focused on atmospheric chlorine. In this study, PM_{2.5} samples were collected from urban and rural sites across China in January 2018, and concentrations of Cl⁻ and other water-soluble ions in PM_{2.5} were analyzed. The size-segregated aerosol Cl⁻ data measured across Chinese cities by other studies were compiled for comparison. The observed data demonstrated that the Cl⁻ concentrations of PM_{2.5} in northern cities ($5.0 \pm 3.7 \mu\text{g}/\text{m}^3$) were higher than those in central ($1.9 \pm 1.2 \mu\text{g}/\text{m}^3$) and southern cities ($0.84 \pm 0.54 \mu\text{g}/\text{m}^3$), suggesting substantial chlorine emissions in northern cities during winter. The concentrations of Cl⁻ in aerosol were significantly higher in urban regions ($0.11\text{--}26.7 \mu\text{g}/\text{m}^3$) compared to than in rural regions ($0.03\text{--}0.61 \mu\text{g}/\text{m}^3$) across China during winter, implying strong anthropogenic chlorine emission in cities. Based on the mole ratios of Cl⁻/Na⁺, Cl⁻/K⁺ and Cl⁻/SO₄²⁻ and the PMF model, Cl⁻ in northern and central cities was mainly sourced from the coal combustion and biomass burning, but in southern cities, Cl⁻ in PM_{2.5} was mainly affected by the equilibrium between gas-phase HCl and particulate Cl⁻. The size-segregated statistical data demonstrated that particulate Cl⁻ had a bimodal pattern, and more Cl⁻ was distributed in the fine model than that in the coarse mode in winter, with the opposite pattern was observed in summer. This may be attributed to both sources of atmospheric Cl⁻ and Cl⁻ involved in chemical processes. This study reports the concentrations of aerosol Cl⁻ on a national scale, and provides important information for modeling the global atmospheric reactive chlorine distribution and the effects of chlorine on atmospheric photochemistry.

Keywords: Cl⁻; PM_{2.5}; spatial distribution; sources; China; winter

1. Introduction

Chlorine is one of the most abundant halogen species in the atmosphere, where it exists as both inorganic Cl (such as particulate Cl⁻ and gas-phase HCl) and organic Cl (such as CH₃Cl and chlorofluorocarbons), and participates in many atmospheric photochemical reactions [1]. Cl⁻-containing inorganic and organic compounds are considered to be one of the factors driving the global climate change [2]. It is well known that halogens decrease the atmospheric ozone concentration [3–7], and that halogens can participate in the NO_x cycle, promoting heterogeneous formation of atmospheric nitrate in both the marine and terrestrial atmospheric boundary layers [8–10]. Using the GEOS-Chem model, halogens were estimated to account for as much as ~15–27% of the global oxidation of volatile organic compounds [7]. In addition, chlorine depletion is a common phenomenon for marine aerosol and the volatilization of gas-phase HCl from the surface of particles

may disturb the aerosol acidity [11–14], which further affects the water-soluble ion concentrations aerosol [15,16]. Although the Cl^- concentration in aerosol has been incidentally reported in many studies, very few studies have paid attention to Cl^- in terrestrial aerosols as compared to marine aerosol, let alone in situ observations on a large spatial scale.

The sources of atmospheric Cl^- have been identified using several different methods, such as determining stable isotopic compositions of Cl^- [17–19], monitoring the relationships between Cl^- and OC, EC, Na^+ , and K^+ [16,20–22], and model simulations [23,24]. Atmospheric Cl^- has many natural sources, including sea water, wildfires, dust storms, and volcanic eruptions [25–28], as well as anthropogenic sources, such as coal combustion, biomass burning, industrial emissions, and the use of sodium chloride on icy roads [20,21,29–35]. The chlorine emissions from sea water (both particulate Cl^- and gas-phase HCl) were estimated to be $1792.6 \text{ Tg Cl yr}^{-1}$ [23], which is considerably higher than emissions from other sources, such as dust (15 Tg Cl yr^{-1} as particulate Cl^-) and volcanic eruptions (2 Tg Cl yr^{-1} as gas-phase HCl) [19]. In terms of anthropogenic sources, the chlorine emission from biomass burning were $6.4 \text{ Tg Cl yr}^{-1}$ [24], which were similar to the emissions of gas phase HCl from coal combustion ($4.6 \text{ Tg Cl yr}^{-1}$, [19]) and urban garbage burning ($6\text{--}9 \text{ Tg Cl yr}^{-1}$, [21]). The majority of atmospheric inorganic chlorine is returned to the Earth's surface by dry or wet deposition. Unlike bioavailable nutrients, such as NO_3^- , that can rapidly affect terrestrial ecosystems [36–39], Cl^- exhibits conservative behavior and very few studies have specifically investigated the influences of atmospheric Cl^- deposition on the biogeochemistry of terrestrial ecosystems [40]. With the high solubility and conservative behavior of Cl^- , the mass balance of Cl^- has been used to evaluate the long-term groundwater recharge of regional hydrologic cycles [41–43]. In addition, studies have demonstrated that deposition of atmospheric Cl^- on the surface of steel may accelerate the corrosion rate and reduce the lifetime of construction steel [44–46]. A review of atmospheric corrosion in China reported that Cl^- plays an important role in the corrosion of metals in areas across China [47].

In this study, $\text{PM}_{2.5}$ samples were collected during January 2018 from 20 cities and 2 rural sites across China (latitude from 22.8° N to 45.7° N and longitude from 102.7° E to 126.7° E ; Figure 1). Concentrations of Cl^- in $\text{PM}_{2.5}$ across Chinese urban and rural sites were measured, aiming to investigate the spatial distribution of Cl^- in $\text{PM}_{2.5}$, and to explore the possible sources of Cl^- in $\text{PM}_{2.5}$ during winter across China. We also summed the size distribution of aerosol Cl^- across China in both winter and summer to examine the seasonal patterns of size-segregated aerosol Cl^- .

2. Materials and Methods

2.1. Sampling and Chemical Analysis

A high-volume total suspended particulate sampler equipped with a $\text{PM}_{2.5}$ impactor (KC-1000; Laoshan Mountain Electronic Instrument Factory Co., Ltd, Qingdao, China) was used to collect $\text{PM}_{2.5}$ samples. The sampling substrate was the Tissuquartz 2500QAT-UP filter (Pall Corp., Port Washington, WA, USA), which was combusted at 450° C for 4 hours before use. The sampling campaigns were taken in January of 2018, and the sampling time for each $\text{PM}_{2.5}$ sample in urban sites was 23.5 hours. According to the latitude distribution and ambient temperature of each sampling sites, the 20 urban sampling sites were divided into three regions: 1) Northern cities (blue solid circles in Figure 1), including Harbin (HRB), Shenyang (SY), Shijiazhuang (SJZ), Tianjin (TJ), Taiyuan (TY), Ji'nan (JN), Qingdao (QD), Xi'an (XA), and Lanzhou (LZ), where regions of heating supply are located in northern China and the average ambient temperature in January is lower than zero. 2) Central cities (yellow solid circles in Figure 1), including Shanghai (SH), Nanjing (NJ), Hangzhou (HZ), Nanchang (NC), Wuhan (WH), Chongqing (CQ) and Chengdu (CD), which are located between 28° N and 32° N , and the average ambient temperature ranges from 2° C to 6° C . 3) Southern cities (red solid circles in Figure 1), including Xiamen (XM), Guangzhou (GZ), Nanning (NN) and Kunming (KM), located south of 25° N where the average ambient temperature is higher than 9° C . We also sampled $\text{PM}_{2.5}$

samples from rural sites (Yudu and Puding, Figure 1), but the sampling time for each PM_{2.5} sample was 47.5 hours and only 16 samples were collected from each rural sites. The latitude distributions of ambient temperature and relative humidity for the urban sites are shown in Figure 1b,c.

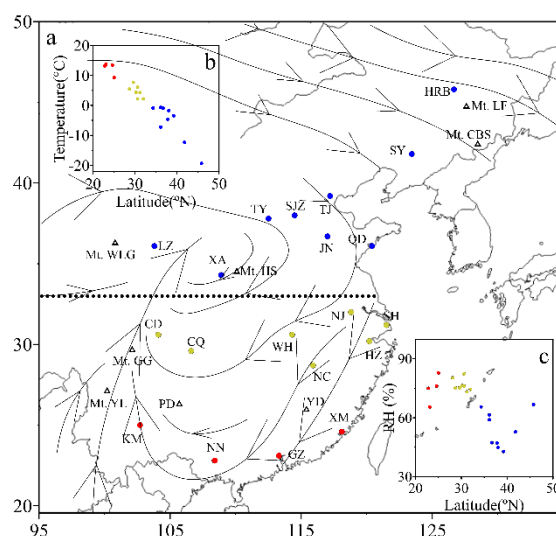


Figure 1. (a) Map of the 25 sampling sites. The color circles and black trigons indicate the urban and rural sites, respectively. The dotted line indicates the boundary line of heating supply in China. The black curve with arrow are the regional wind streamlines at 1000 hPa during the Asian winter monsoon period based on the National Center for Environmental Prediction (NCEP) dataset. (b) Scatter plot of average temperature against latitude for urban sampling sites. (c) Scatter plot of average relative humidity (RH) against latitude for urban sampling sites. The data of temperature and RH are from <http://www.weatherandclimate.info/archive.php>.

The water-soluble ions analyzing processes can be referenced to Luo et al. [16] and Hsu et al. [48]. Briefly, a one-eighth piece of filter was extracted with 50 mL of Milli-Q water (conductivity 18.2 MΩ/cm) in a clear centrifuge tube. The centrifuge tube filled with filter and 50 mL Milli-Q water, was subjected to ultrasonically extraction for 30 minutes under room temperature, then centrifuged for 20 minutes at 2000 revolutions per minute. Finally, the extract was filtered using a 0.22 μm Millipore syringe filter. After filtering, the extract was stored at −20 °C for further chemical analysis. The water-soluble ions (Cl^- , NH_4^+ , Na^+ , Mg^{2+} , K^+ , Ca^{2+} , NO_3^- , and SO_4^{2-}) were analyzed by a ion chromatograph (Thermo Fisher Scientific, Inc., Waltham, MA, USA). For the urban samples, all of the above ions were analyzed, but for the rural sites, only anions (Cl^- , NO_3^- and SO_4^{2-}) were analyzed.

2.2. Model of Positive Matrix Factorization

The positive matrix factorization (PMF 5.0) is a factor-based receptor model used for quantifying the contribution of sources to samples based on the fingerprints of the sources [49]. In this study, 270 × 8 matrix (sample number × 8 species) date sets for northern cities, 214 × 8 matrix date sets for central cities and 156 × 8 matrix date sets for southern cities were introduced into the PMF 5.0 to quantify sources of Cl^- in PM_{2.5} across China during the winter. We ran PMF 5.0 with the number of runs set to 20 and the number of factors set from 3 to 6, and examined Q (Robust)/Qexp to choose the best number of factors for the model. The detailed model parameter settings can be found in the user guide (www.epa.gov) and other studies [50,51].

3. Results and Discussions

3.1. Spatial Distributions of Cl^- , SO_4^{2-} , K^+ and Na^+ in $\text{PM}_{2.5}$

Overall, the Cl^- concentrations in $\text{PM}_{2.5}$ ranged from 0.11 to 26.7 $\mu\text{g}/\text{m}^3$ over the 20 urban sites (Table 1; Figure 2a), which is consistent with previous observations of aerosol Cl^- concentrations across China during winter [52–55]. The concentrations of Cl^- in $\text{PM}_{2.5}$ across Chinese cities in our observations were significantly higher than previous studies of aerosol Cl^- during wintertime in the northeastern United States (0.06–0.23 $\mu\text{g}/\text{m}^3$) [14], in Iasi ($0.32 \pm 0.15 \mu\text{g}/\text{m}^3$) [30], and in Sao Paulo (1.4 $\mu\text{g}/\text{m}^3$) [56], suggesting intensive inorganic chlorine emissions in China. The aerosol Cl^- concentrations in rural sites ranged from $0.07 \pm 0.02 \mu\text{g}/\text{m}^3$ to $0.55 \pm 0.19 \mu\text{g}/\text{m}^3$ across China during winter (Table 2, Figure 2b), which were significantly lower than those in urban sites (Table 1; Figure 2a), suggesting strong anthropogenic emissions of chlorine in urban sites. In addition, there were large spatial variations in aerosol Cl^- in urban and rural sites. For example, the average Cl^- concentration ($9.81 \pm 5.20 \mu\text{g}/\text{m}^3$) in $\text{PM}_{2.5}$ observed in Shijiazhuang (located in northern China) was thirteen-fold times higher than those ($0.69 \pm 0.31 \mu\text{g}/\text{m}^3$) occurred in Kunming (located in southwest China) during winter (Table 1). The average concentration of aerosol Cl^- sampled in Changbai Mountain ($0.39 \pm 0.15 \mu\text{g}/\text{m}^3$) was five times higher than that ($0.07 \pm 0.02 \mu\text{g}/\text{m}^3$) the rural site of Yudu (Table 2).

Table 1. Concentrations of Cl^- in urban $\text{PM}_{2.5}$ ($\mu\text{g}/\text{m}^3$) across China in January 2018.

Locations	Min	Max	Median	Mean ¹	Mean ²	Mean ³	SD
Harbin (HRB)	1.15	18.6	6.77	6.91	5.78	6.65	3.94
Shenyang (SY)	1.00	7.24	3.57	3.73	3.34	3.72	1.69
Tianjin (TJ)	0.39	16.4	4.30	5.29	4.19	5.24	3.53
Shijiazhuang (SJZ)	1.29	26.7	9.46	9.81	8.44	9.7	5.20
Taiyuan (TY)	1.21	12.4	5.98	6.37	5.38	6.3	3.48
Ji'nan (JN)	0.84	10.44	3.12	3.79	3.21	3.64	2.36
Qingdao (QD)	0.99	9.77	2.65	3.18	2.74	3.17	1.95
Xi'an (XA)	1.08	10.5	3.18	3.80	3.34	3.74	2.14
Lanzhou (LZ)	0.67	5.23	2.73	2.62	2.27	2.61	1.30
Shanghai (SH)	0.17	5.61	1.30	1.73	1.29	1.73	1.41
Nanjing (NJ)	0.69	5.83	2.11	2.30	2.05	2.29	1.14
Hangzhou (HZ)	0.42	4.75	1.91	1.94	1.55	1.92	1.24
Nanchang (NC)	0.27	3.37	0.95	1.13	0.90	1.05	0.79
Wuhan (WH)	0.28	4.60	2.12	2.27	2.07	2.13	0.88
Chongqing (CQ)	0.32	6.14	1.56	1.73	1.28	1.72	1.34
Chengdu (CD)	0.42	4.52	2.39	2.32	1.96	2.32	1.17
Kunming (KM)	0.26	1.55	0.63	0.69	0.63	0.69	0.31
Nanning (NN)	0.24	2.63	0.78	0.90	0.76	0.90	0.54
Guangzhou (GZ)	0.11	1.83	0.66	0.76	0.59	0.76	0.52
Xiamen (XM)	0.13	4.02	0.93	1.01	0.83	1.01	0.70

¹ Arithmetic mean, ² Geometric mean, ³ Volume mean.

The Cl^- concentrations in $\text{PM}_{2.5}$ gradually decreased from the northern cities ($5.0 \pm 3.7 \mu\text{g}/\text{m}^3$) to the central cities ($1.9 \pm 1.2 \mu\text{g}/\text{m}^3$), and then to the southern cities ($0.84 \pm 0.54 \mu\text{g}/\text{m}^3$) across China during winter (Figure 3a). Similar aerosol Cl^- spatial patterns were also seen for the rural sites over China (Figure 2b). These results indicated a national pattern of aerosol Cl^- across China in winter. Moreover, the decreased concentrations of aerosol Cl^- , along with the path of the Asian winter monsoon from the northern to southern China, suggested that the atmospheric chlorine may be transported along the wind field. Although ambient temperature and RH have an obvious latitude distribution from north to south China (Figure 1b,c), there were no positive or negative correlations between aerosol Cl^- and temperature, and between aerosol Cl^- and RH for all the study regions. In addition, the observations of Cl^- concentrations were not consistent with the spatial distribution of the emission of

chlorine ($\text{HCl} + \text{Cl}_2$) modeled by the coal consumption and chlorine content of coal in each province for the whole year of 2012 [57]. Liu et al. showed that high chlorine emissions are mainly distributed in the Sichuan Basin, the Yangtze River Delta and the North China Plain, with no latitude variations across China [57]. Due to a lack of coal consumption in January 2018 for the observed cities, we cannot estimate the chlorine emissions from coal combustion. The discrepancies between the observed aerosol Cl^- concentrations and the modelled chlorine emissions across China may be related to the seasonal differences (for example higher chlorine in winter than summer [58]), and the study scale differences (for example, our study focused on the cities, but the study of Liu et al. [57] including both cities and countryside).

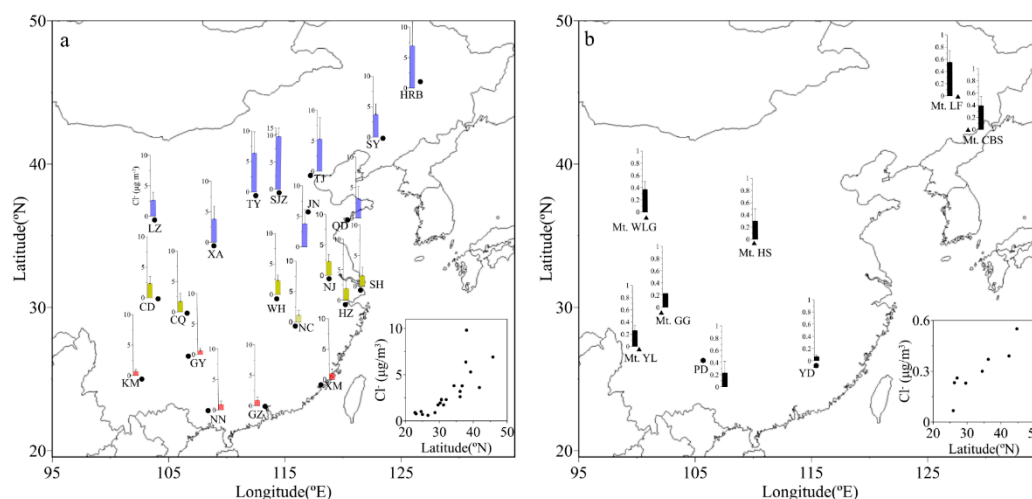


Figure 2. Concentration distribution of Cl^- in $\text{PM}_{2.5}$ sampled in urban sites (a: the data from Table 1) and rural sites (b: the data from Table 2) in January 2018.

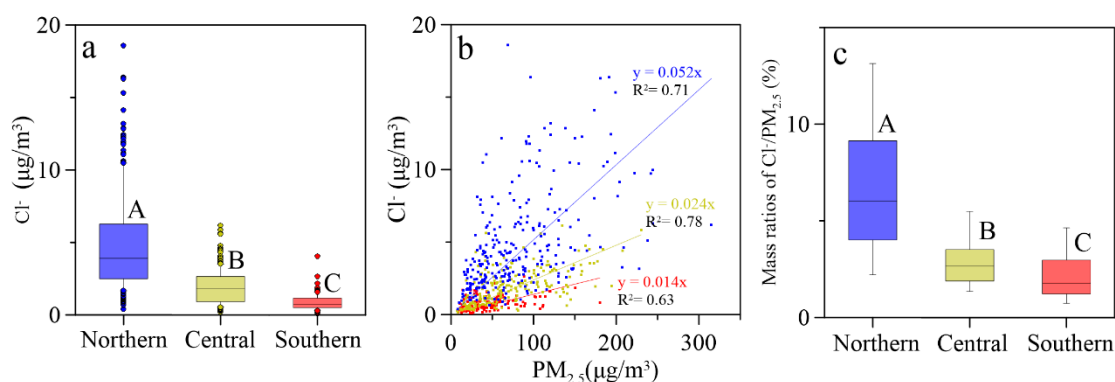


Figure 3. Concentrations of Cl^- (a), scatter plot of concentration of Cl^- against with $\text{PM}_{2.5}$ (b) and mass ratios of $\text{Cl}^-/\text{PM}_{2.5}$ (c) in northern, central and southern cities, respectively. The large boxes in (a) and (c) represent the interquartile range from the 25th to 75th percentile. The line inside the box indicates the median value. The whiskers extend upward to the 90th and downward to the 10th percentile. Significant differences at the $p < 0.05$ level among different regions are marked with uppercase letters.

In addition, there was a positive relationship between concentrations of Cl^- and $\text{PM}_{2.5}$ in northern China ($R^2 = 0.71$), central China ($R^2 = 0.78$) and southern China ($R^2 = 0.63$) (Figure 3b), which indicated that Cl^- accumulates as concentration of particulate matter increases. The average mass ratios of $\text{Cl}^-/\text{PM}_{2.5}$ in northern cities ($6.0 \pm 4.8\%$) were higher than those in central cities ($2.7 \pm 2.1\%$) and southern cities ($1.8 \pm 1.8\%$) (Figure 3c), and were also higher than previous studies (ranging from 0.34 to 4.55) [54,58]. The anomalous high mass ratios of $\text{Cl}^-/\text{PM}_{2.5}$ in northern cities may be connected with the high emission of anthropogenic chlorine [58], or with the higher gas-phase HCl partition into

particulate Cl^- [57], or with the implementation of air pollutant emission reduction measures, which dropped the concentrations of $\text{PM}_{2.5}$ during this study period. Such high mass ratios of $\text{Cl}^-/\text{PM}_{2.5}$ in widespread northern cities deserve further explanation.

Table 2. Concentrations of aerosol Cl^- in rural sites ($\mu\text{g}/\text{m}^3$) during winter.

Locations	Types	Min	Max	Mean	SD	References
Yudu (YD)	$\text{PM}_{2.5}$	0.03	0.11	0.07	0.02	This study
Puding (PD)	$\text{PM}_{2.5}$	0.03	0.61	0.23	0.19	This study
Mt. Hua (HS)	PM_{10}			0.3	0.2	[59]
Mt. Yulong (YL)	TSP	0.13	0.46	0.26	0.08	[60]
Mt. Gongga (GG)	$\text{PM}_{2.5}$	0.03	0.52	0.17	-	[61]
Mt. Gongga (GG)	PM_{10}	0.05	1.13	0.26	-	[61]
Mt. changbai (CBS)	$\text{PM}_{2.5}$	-	-	0.39	0.15	[62]
Mt. Longfeng (LF)	TSP	-	-	0.55	0.19	[63]
Mt. Waliguan (WLG)	TSP	-	-	0.37	0.13	[63]

Concentrations of SO_4^{2-} , K^+ and Na^+ also decreased from the northern cities to the southern cities (Figure 4). These results, on the one hand, validate our regional divisions (i.e., northern, central and southern cities), but on the other hand, imply that the strongest anthropogenic emission of SO_4^{2-} , K^+ and Na^+ occurred in northern China. Most urban aerosol SO_4^{2-} is associated with the coal combustion [20,22]. The highest concentration of SO_4^{2-} in $\text{PM}_{2.5}$ in northern cities ($13.3 \pm 9.0 \mu\text{g}/\text{m}^3$) in these measurements (Figure 4a) may be attributed to increasing consumption of coal in winter for heating supply. The SO_4^{2-} in central cities ($11.7 \pm 6.7 \mu\text{g}/\text{m}^3$) may be sourced from the local emissions or transport from the northern China. High K^+ emission is a characteristic of biomass burning [64,65]. In these observed campaigns, the highest concentration of K^+ occurred in northern cities ($0.98 \pm 0.78 \mu\text{g}/\text{m}^3$), followed by central cities ($0.77 \pm 0.52 \mu\text{g}/\text{m}^3$), and then southern cities ($0.59 \pm 0.48 \mu\text{g}/\text{m}^3$) (Figure 4b). However, the active fire points from the Aqua and Terra MODIS data in January 2018 displayed an opposite trend for K^+ , i.e., less fire points in northern China but more in southern China (Figure 5). For the highest concentrations of K^+ in northern China, we speculate that coal combustion may be an important source of K^+ [64,66], but the contribution from residential biofuel combustion may not be negligible [58]. In southern China, K^+ may be mainly from the biomass burning (Figure 5). Significantly higher Na^+ in northern cities ($0.75 \pm 0.58 \mu\text{g}/\text{m}^3$) compared to central ($0.26 \pm 0.19 \mu\text{g}/\text{m}^3$) and southern ($0.21 \pm 0.16 \mu\text{g}/\text{m}^3$) cities (Fig. 4c) further indicated that there is higher consumption of coal in northern cities, as Na^+ emission is a characteristic of coal combustion [67,68].

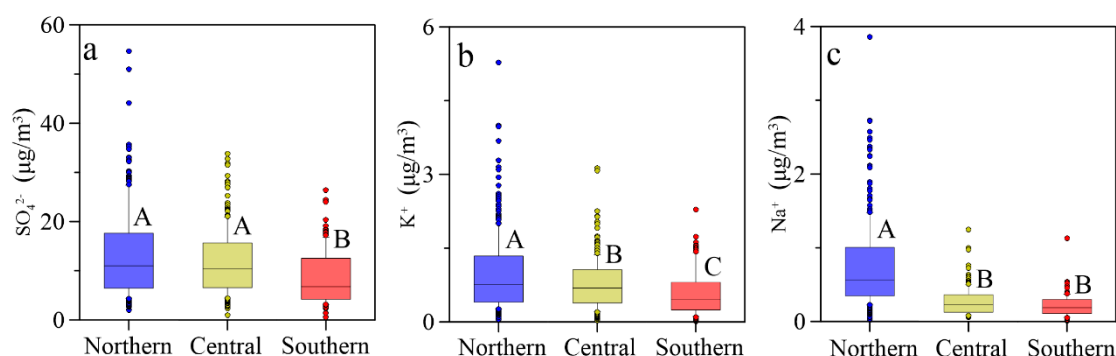


Figure 4. Concentrations of SO_4^{2-} (a), K^+ (b) and Na^+ (c) in northern, central and southern cities, respectively. The large boxes represent the interquartile range from the 25th to 75th percentile. The line inside the box indicates the median value. The whiskers extend upward to the 90th and downward to the 10th percentile. Significant differences at the $p < 0.05$ level among different regions are marked with uppercase letters.

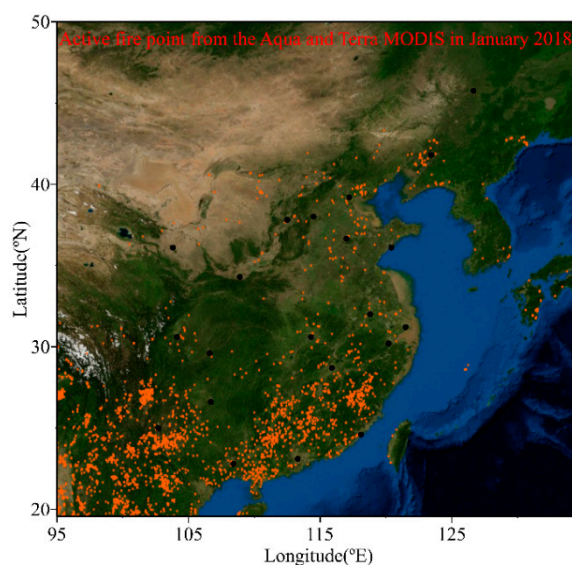


Figure 5. Active fire point across China from Aqua and Terra MODIS data in January 2018.

3.2. Source Apportionment of Cl^- in $\text{PM}_{2.5}$

To explore the possible sources of Cl^- in $\text{PM}_{2.5}$ over Chinese cities in winter, the mole ratios of Cl^-/Na^+ , Cl^-/K^+ and $\text{Cl}^-/\text{SO}_4^{2-}$, and the PMF 5.0 model, were employed to explore and estimate the origins of Cl^- . The mole ratios of Cl^-/Na^+ were 5.5 ± 3.8 , 5.5 ± 2.5 and 4.5 ± 3.9 in northern, central and southern cities (Figure 6a), respectively, which were significantly higher than sea water (1.17) [69]. Even for coastal cities, the average ratios of Cl^-/Na^+ were (5.5 ± 3.1 in northern cities (TJ and QD), 4.7 ± 2.8 in central cities (SH and HZ) and 2.9 ± 2.5 in southern cities (XM and GZ)), which were still higher than seawater. These results indicate that the oceanic source of chlorine is minor for all observed inland cities. Moreover, the mole ratios of Cl^-/Na^+ in $\text{PM}_{2.5}$ were higher than that (1.3 ± 0.87) in urban dust [70], implying the urban dust source of chlorine is also minor for atmospheric aerosol chlorine. For the aerosol chlorine in an urban atmosphere, excluding the natural origins, anthropogenic emissions (such as coal combustion and biomass burning (including burning of residential and industrial biofuel, agricultural waste and wildfires)) have been widely mentioned in the literature [32,57,58]. However, the mole ratios of Cl^-/Na^+ in $\text{PM}_{2.5}$ for all the cities in our observations during winter were higher than the Cl^-/Na^+ mole ratios in $\text{PM}_{2.5}$ that collected directly from the flue gas of biomass burning (3.2 ± 2.7) [71–74] and coal combustion (1.2 ± 1.9) [73,75–79] (Figure 6a). This may be ascribed to, on the one hand, the chlorine released from biomass burning and coal combustion, including both gas-phase HCl and particulate Cl^- [76], and sampling the $\text{PM}_{2.5}$ from the flue gas only, which would filter the particulate Cl^- . On the other hand, Cl^- sampled in urban $\text{PM}_{2.5}$ not only involves the primary particulate Cl^- , but also contains the transformation of gas-phase HCl to particulate Cl^- [14].

The lower molar ratios of Cl^-/K^+ from the flue gas of biomass burning than coal combustion (Figure 6b), agrees with the relatively high potassium released from the biomass burning [64,65] and implies that more chlorine is released from coal combustion than biomass burning. High Cl^-/K^+ ratios in northern cities (Figure 6b), together with high concentrations of Cl^- and K^+ in northern cities (Figures 3a and 4b), suggests that chlorine is mainly related to potassium in $\text{PM}_{2.5}$. Moreover, the lower Cl^-/K^+ ratios in southern cities, coupled with the lower concentrations of Cl^- and K^+ in southern cities, suggests that more K^+ than Cl^- is emitted, which is consistent with the more active fire points in southern China than central and northern China (Figure 5). Furthermore, the well correlation coefficients (0.78) between Cl^- and K^+ in northern cities implies that there are similar sources of Cl^- and K^+ . These results suggested that Cl^- and K^+ in northern cities is mainly sourced from the coal combustion. A significantly higher $\text{Cl}^-/\text{SO}_4^{2-}$ ratio from biomass burning than coal combustion

indicates that there is relatively high Cl^- emission from the biomass burning (Figure 6c). The decreasing trend in the $\text{Cl}^-/\text{SO}_4^{2-}$ ratio from the northern cities to the southern cities (Figure 6c) suggests that the contribution of biomass burning to aerosol Cl^- cannot be neglected in northern cities. Similarly, coal combustion also may be an important source of aerosol Cl^- in central and southern cities.

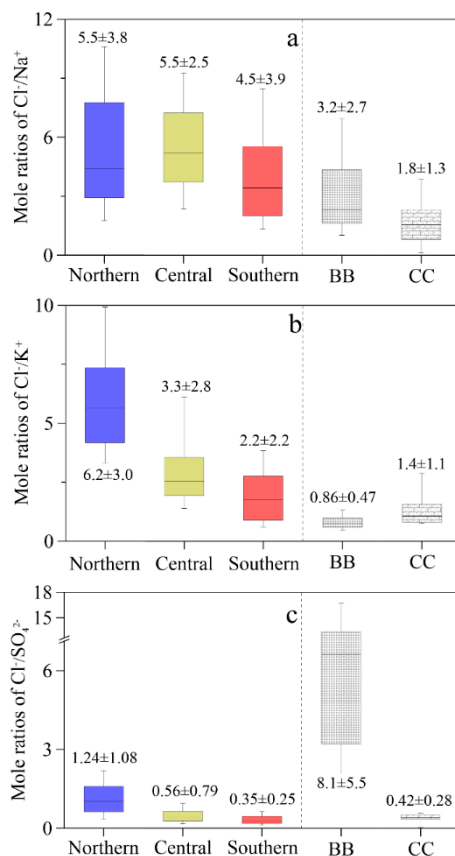


Figure 6. Mole ratios of Cl^-/Na^+ (a), Cl^-/K^+ (b) and $\text{Cl}^-/\text{SO}_4^{2-}$ (c) in aerosol collected from the northern, central and southern cities, and from the gas flue directly from biomass burning (BB) and coal combustion (CC).

To quantify the possible contributions of different sources of Cl^- in $\text{PM}_{2.5}$, four resolved source profiles for Cl^- and other water-soluble ions in $\text{PM}_{2.5}$ were performed by the PMF model (Figure 7). The first factor with high loading of K^+ indicated the sources of coal combustion and biomass burning. The second factor was characterized by high amounts of secondary formation ions (NO_3^- , SO_4^{2-} and NH_4^+), giving the secondary formation source. A high Ca^{2+} level indicated that the third factor was related to the soil dust. The fourth factor showed a high amount of Na^+ , which may be associated with the sea salts or with sodium-containing salts in urban spray water (hereafter, 'salts' includes both sodium-containing salts in spray water and sea salts). In order to improve the urban air quality, water is frequently sprayed into the air by a sprinkler in many Chinese cities, governed by the local government. The mode results showed that the dominant contribution of Cl^- in $\text{PM}_{2.5}$ was from coal combustion and biomass burning, and the soil dust and salts were the other contributors in northern cities (Figure 7, Panel A). In central cities, 60% of Cl^- in $\text{PM}_{2.5}$ is from coal combustion and biomass burning, but the remainder is from the salts (Figure 7, Panel B). However, in southern cities, around 60% of Cl^- in $\text{PM}_{2.5}$ is associated with the secondary formation ions (Figure 7, Panel C), implying an abundant partition of gas-phase chlorine into particulate Cl^- .

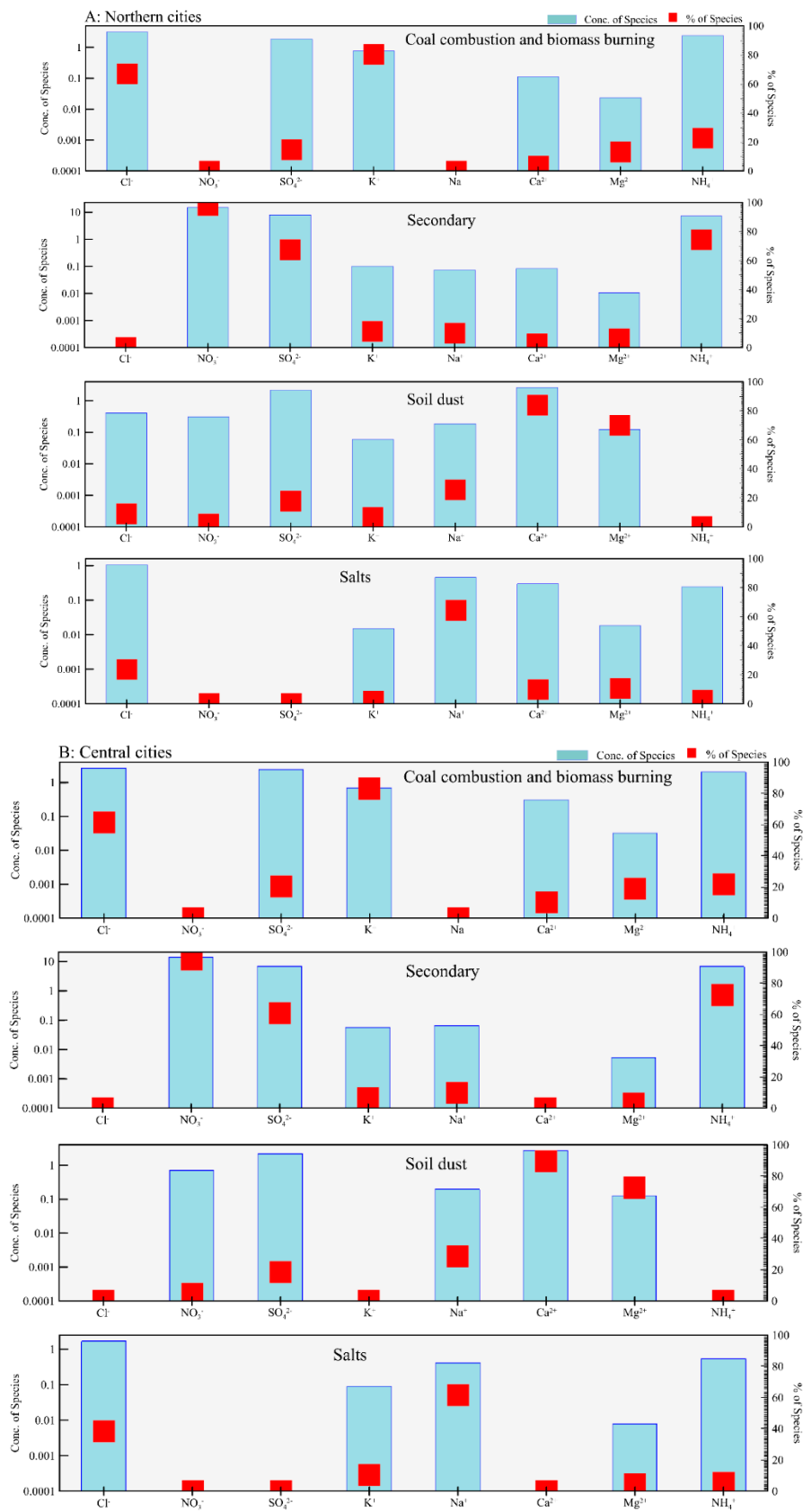


Figure 7. Cont.

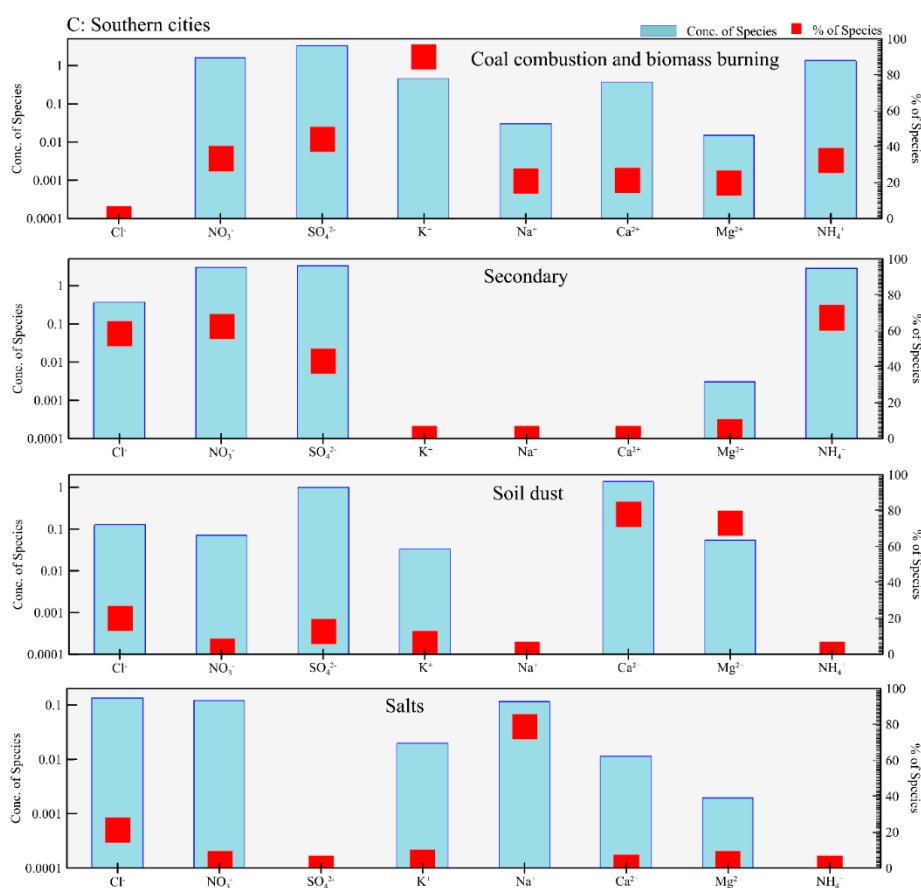


Figure 7. Source profiles of chlorine and other water-soluble ions deduced from the PMF5.0 analysis in northern (Panel A), central (Panel B) and southern (Panel C) cities.

3.3. Size Distributions of Aerosol Cl⁻: A Review

Here, the published datasets of size-segregated urban aerosol Cl⁻ that were sampled during both winter and summer in China were compiled for comparison [30,52,56,80–87] (Figure 8). The compiled size distribution results of aerosol Cl⁻ displayed a bimodal pattern, with peaks located between 0.43–0.65 μm for fine mode particles and 4.7–5.8 μm for coarse mode particles both in winter (Figure 8a) and summer (Figure 8b). The dual peak distribution of aerosol Cl⁻ might be ascribed to both the sources of chlorine and the gas-particle partitioning of chlorine. The sources of aerosol Cl⁻ in the urban atmosphere include primary particulate Cl⁻ emission (particulate Cl⁻ directly emitted from the coal combustion, biomass burning, mineral dust and sea salts) and the transformation of gas-phase HCl (mainly emitted from the coal combustion, biomass burning and industrial emissions) into particulate Cl⁻ [21,32,67]. The primary particulate Cl⁻ sources, such as sea salt and mineral dust, were mainly distributed in the coarse mode. For example, Cl⁻ in aerosols that were sampled in the open ocean was dominantly distributed in size ranges from 4.7 to 5.8 μm [88], and during dust periods, aerosol Cl⁻ was mainly located in the coarse mode [89]. Primary particulate Cl⁻ emitted directly from coal combustion and biomass burning was distributed in the fine mode [34,75]. However, most of the chlorine was emitted into the atmosphere from coal combustion and biomass burning as gas-phase HCl [90,91]. The equilibrium of gas-phase HCl and particulate Cl⁻ may affect the size distribution of aerosol Cl⁻. Previous studies have shown that the partitioning of gas-phase HCl and particulate Cl⁻ depends on particulate pH, atmospheric relative humidity, ambient temperature, particle loading and particle water content [14,30]. Thus, it is hard to discuss the size distributions of aerosol Cl⁻ during gas-particle partitioning of chlorine for the in-situ observations. In addition, the neutral reaction between gas-phase HCl and mineral particles may enhance the Cl⁻ distribution in coarse

mode particles [26], and the reaction of gas-phase HCl with NH_3 to form solid NH_4Cl is located in the fine mode [31].

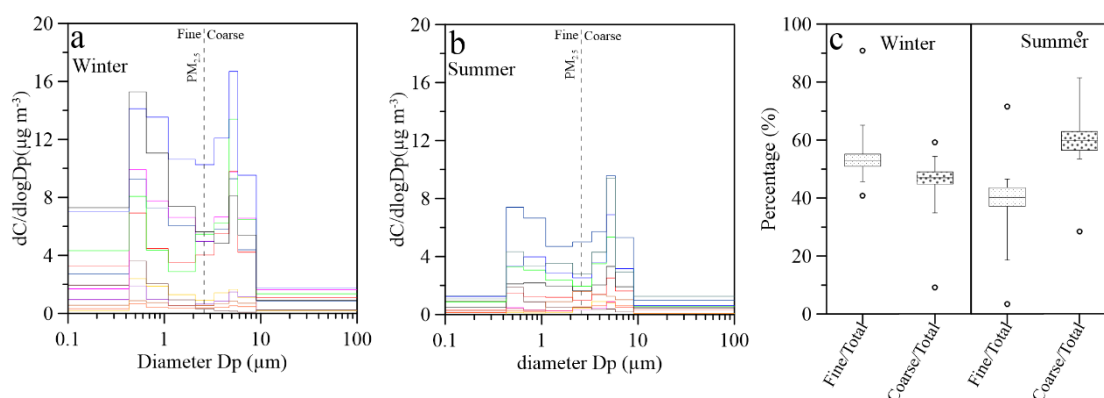


Figure 8. Size distributions of Cl^- -containing aerosol particles in winter (a) and summer (b) in China. (c) The mass ratios of Cl^- in fine and coarse particles during winter and summer using the data from (a) and (b).

The statistical results also showed that urban aerosol Cl^- concentration distributed in the fine mode was similar to that in the coarse mode during winter, but significantly higher Cl^- concentration was distributed in the coarse mode than in the fine mode during summer (Figure 8c). The seasonal discrepancies in size-segregated aerosol Cl^- concentration may be attributed to several possible factors. First, during summer, the prevailing wind direction is from the ocean to the land, which may carry the sea salt into the inland, which may enhance aerosol Cl^- in the coarse mode. On the contrary, during winter, the wind direction of the Asian winter monsoon is from the land to the ocean, which weakens the influences of sea salt. Second, more coal and biomass consumption for heating occurs in winter than summer in northern China, which may enhance the primary fine mode aerosol Cl^- during winter. Third, concentrations of $\text{PM}_{2.5}$ are generally higher in winter than summer [92], and fine particles provide a relatively large specific surface area, which may enhance Cl^- in the fine mode in winter [31]. Fourth, acidic ions, such as SO_4^{2-} and NO_3^- , distributed in the fine mode [52,85], can acidize fine mode aerosols [93]. In summer, strong solar irradiation can enhance gas-phase HCl release from the acidic fine particles through acid displacement between sulfuric acid or nitric acid and deliquesced Cl^- ($\text{HNO}_3(\text{g}) + \text{Cl}^-(\text{aq}) \rightarrow \text{NO}_3^-(\text{aq}) + \text{HCl}(\text{g})$ or $\text{H}_2\text{SO}_4(\text{g}) + \text{Cl}^-(\text{aq}) \rightarrow \text{SO}_4^{2-}(\text{aq}) + \text{HCl}(\text{g})$) [89]. On the contrary, more Cl^- may reside in fine mode aerosol in winter than summer.

4. Conclusions

Samples of $\text{PM}_{2.5}$ were collected from 20 urban and two rural sites across China during winter, and the water-soluble ions were analyzed. The aerosol Cl^- concentrations decreased from northern to southern China, both in urban cities and rural sites, indicating a national spatial pattern of aerosol Cl^- during winter across China. The high concentration of Cl^- in northern China, coupled with the high concentrations of SO_4^{2-} , K^+ and Na^+ and the high mole ratios of Cl^-/Na^+ , Cl^-/K^+ and $\text{Cl}^-/\text{SO}_4^{2-}$ in northern cities, suggests that coal combustion and biomass burning are the dominate sources of Cl^- in $\text{PM}_{2.5}$. However, for the southern cities, the Cl^- in $\text{PM}_{2.5}$ was mainly affected by partition of gas-phase chlorine to particulate Cl^- . Statistical analysis of the size distributions of Cl^- -containing aerosols exhibited a bimodal pattern during both winter and summer. This bimodal pattern may be attributed to chlorine sources, Cl^- involved photochemical reactions and partition of gas-phase chlorine to particulate Cl^- . Our simultaneously in-situ observations of Cl^- concentrations in $\text{PM}_{2.5}$ across China provides information for accurately modeling the spatial distribution of atmospheric chlorine and its effect on atmospheric photochemistry.

Author Contributions: Conceptualization, L.L., H.-Y.X. and H.-W.X.; methodology, Y.-Y.Z., Z.-Y.Z., N.-J.Z., C.L., and Y.-J.X.; software, L.L.; validation, L.L. and H.-Y.X.; formal analysis, L.L.; writing—original draft preparation, L.L. and Y.-Y.Z.; writing—review and editing, L.L. and H.-Y.X.; supervision, H.-Y.X. and H.-W.X.

Funding: This research was supported by the National Natural Science Foundation of China (41425014 and 41763001), Doctoral Scientific Research Foundation of the East China University of Technology (DHBK2016105), Science and Technology Project of the Jiangxi Provincial Department of Education (GJJ160580), and the Scientific Research Foundation of the East China University of Technology for the Science and Technology Innovation Team (DHKT2015101).

Conflicts of Interest: The authors declare no conflict of interest.

References

1. Seinfeld, J.H.; Pandis, S.N. *Atmospheric Chemistry and Physics: From Air Pollution to Climate Change*, 2nd ed.; John Wiley & Sons, Inc.: New York, NY, USA, 2016.
2. IPCC. *Climate Change 2013: The Physical Science Basis*; Cambridge University Press: Cambridge, UK, 2013.
3. Hönninger, G.; Platt, U. Observations of BrO and its vertical distribution during surface ozone depletion at Alert. *Atmos. Environ.* **2002**, *36*, 2481–2489. [[CrossRef](#)]
4. Sarwar, G.; Gantt, B.; Schwede, D.; Foley, K.; Mathur, R.; Saiz-Lopez, A. Impact of Enhanced Ozone Deposition and Halogen Chemistry on Tropospheric Ozone over the Northern Hemisphere. *Environ. Sci. Technol.* **2015**, *49*, 9203–9211. [[CrossRef](#)] [[PubMed](#)]
5. Simpson, W.R.; Von Glasow, R.; Riedel, K.; Anderson, P.; Ariya, P.; Bottenheim, J.; Burrows, J.; Carpenter, L.J.; Fries, U.; Goodsite, M.E.; et al. Halogens and their role in polar boundary-layer ozone depletion. *Atmos. Chem. Phys.* **2007**, *7*, 4375–4418. [[CrossRef](#)]
6. Saiz-Lopez, A.; Von Glasow, R. Reactive halogen chemistry in the troposphere. *Chem. Soc. Rev.* **2012**, *41*, 6448–6472. [[CrossRef](#)] [[PubMed](#)]
7. Sherwen, T.; Schmidt, J.A.; Evans, M.J.; Carpenter, L.J.; Großmann, K.; Eastham, S.D.; Jacob, D.J.; Dix, B.; Koenig, T.K.; Sinreich, R.; et al. Global impacts of tropospheric halogens (Cl, Br, I) on oxidants and composition in GEOS-Chem. *Atmos. Chem. Phys.* **2016**, *16*, 12239–12271. [[CrossRef](#)]
8. Ahern, A.T.; Goldberger, L.; Jahl, L.; Thornton, J.; Sullivan, R.C. Production of N₂O₅ and ClNO₂ through Nocturnal Processing of Biomass-Burning Aerosol. *Environ. Sci. Technol.* **2018**, *52*, 550–559. [[CrossRef](#)] [[PubMed](#)]
9. Morin, S.; Savarino, J.; Frey, M.M.; Yan, N.; Bekki, S.; Bottenheim, J.W.; Martins, J.M.F. Tracing the Origin and Fate of NO_x in the Arctic Atmosphere Using Stable Isotopes in Nitrate. *Science* **2008**, *322*, 730–732. [[CrossRef](#)] [[PubMed](#)]
10. Altieri, K.E.; Hastings, M.G.; Gobel, A.R.; Peters, A.J.; Sigman, D.M. Isotopic composition of rainwater nitrate at Bermuda: The influence of air mass source and chemistry in the marine boundary layer. *J. Geophys. Res. Atmos.* **2013**, *118*, 11304–11316. [[CrossRef](#)]
11. Keene, W.C.; Savoie, D.L. The pH of deliquesced sea-salt aerosol in polluted marine air. *Geophys. Res. Lett.* **1998**, *25*, 2181–2184. [[CrossRef](#)]
12. Von Glasow, R.; Sander, R. Variation of sea salt aerosol pH with relative humidity. *Geophys. Res. Lett.* **2001**, *28*, 247–250. [[CrossRef](#)]
13. Zhao, Y.; Gao, Y. Acidic species and chloride depletion in coarse aerosol particles in the US east coast. *Sci. Total Environ.* **2008**, *407*, 541–547. [[CrossRef](#)]
14. Haskins, J.D.; Jaeglé, L.; Shah, V.; Lee, B.H.; Lopez-Hilfiker, F.D.; Campuzano-Jost, P.; Schroder, J.C.; Day, D.A.; Guo, H.; Sullivan, A.P.; et al. Wintertime Gas-Particle Partitioning and Speciation of Inorganic Chlorine in the Lower Troposphere Over the Northeast United States and Coastal Ocean. *J. Geophys. Res. Atmos.* **2018**, *123*, 12897–12916. [[CrossRef](#)]
15. Sasakawa, M.; Uematsu, M. Relative contribution of chemical composition to acidification of sea fog (stratus) over the northern North Pacific and its marginal seas. *Atmos. Environ.* **2005**, *39*, 1357–1362. [[CrossRef](#)]
16. Luo, L.; Yao, X.H.; Gao, H.W.; Hsu, S.C.; Li, J.W.; Kao, S.J. Nitrogen speciation in various types of aerosols in spring over the northwestern Pacific Ocean. *Atmos. Chem. Phys.* **2016**, *16*, 325–341. [[CrossRef](#)]
17. Volpe, C.; Spivack, A.J.; Wahlen, M.; Pszenny, A.A.P. Chlorine isotopic composition of marine aerosols: Implications for the release of reactive chlorine and HCl cycling rates. *Geophys. Res. Lett.* **1998**, *25*, 3831–3834. [[CrossRef](#)]

18. Koehler, G.; Wassenaar, L.I. The stable isotopic composition ($^{37}\text{Cl}/^{35}\text{Cl}$) of dissolved chloride in rainwater. *Appl. Geochem.* **2010**, *25*, 91–96. [[CrossRef](#)]
19. Keene, W.C.; Khalil, M.A.K.; Erickson, D.J.; McCulloch, A.; Graedel, T.E.; Lobert, J.M.; Aucott, M.L.; Gong, S.L.; Harper, D.B.; Kleiman, G.; et al. Composite global emissions of reactive chlorine from anthropogenic and natural sources: Reactive Chlorine Emissions Inventory. *J. Geophys. Res. Space Phys.* **1999**, *104*, 8429–8440. [[CrossRef](#)]
20. Zhang, R.; Jing, J.; Tao, J.; Hsu, S.-C.; Wang, G.; Cao, J.; Lee, C.S.L.; Zhu, L.; Chen, Z.; Zhao, Y. Chemical characterization and source apportionment of PM_{2.5} in Beijing: Seasonal perspective. *Atmos. Chem. Phys.* **2013**, *13*, 7053–7074. [[CrossRef](#)]
21. Christian, T.J.; Yokelson, R.J.; Cárdenas, B.; Molina, L.T.; Engling, G.; Hsu, S.-C. Trace gas and particle emissions from domestic and industrial biofuel use and garbage burning in central Mexico. *Atmos. Chem. Phys.* **2010**, *10*, 565–584. [[CrossRef](#)]
22. Luo, L.; Wu, Y.; Xiao, H.; Zhang, R.; Lin, H.; Zhang, X.; Kao, S.-J. Origins of aerosol nitrate in Beijing during late winter through spring. *Sci. Total Environ.* **2019**, *653*, 776–782. [[CrossRef](#)]
23. Seuzaret, C.; Gong, S.L.; Erickson, D.J.; Keene, W.C. A general circulation model based calculation of HCl and ClNO₂ production from sea salt dechlorination: Reactive Chlorine Emissions Inventory. *J. Geophys. Res. Space Phys.* **1999**, *104*, 8347–8372. [[CrossRef](#)]
24. Lobert, J.M.; Yevich, R.; Keene, W.C.; Logan, J.A. Global chlorine emissions from biomass burning: Reactive Chlorine Emissions Inventory. *J. Geophys. Res. Space Phys.* **1999**, *104*, 8373–8389. [[CrossRef](#)]
25. Liss, P.S.; Johnson, M.T. *Ocean-Atmosphere Interactions of Gases and Particles*; Springer: Heidelberg, Germany; New York, NY, USA; Dordrecht, Netherlands; London, UK, 2014.
26. Zhang, X.; Zhuang, G.; Yuan, H.; Rahn, K.A.; Wang, Z.; An, Z. Aerosol Particles from Dried Salt-Lakes and Saline Soils Carried on Dust Storms over Beijing. *Terr. Atmos. Ocean. Sci.* **2009**, *20*, 6. [[CrossRef](#)]
27. Delmelle, P.; Stix, J.; Bourque, C.P.-A.; Baxter, P.J.; Garcia-Alvarez, J.; Barquero, J. Dry Deposition and Heavy Acid Loading in the Vicinity of Masaya Volcano, a Major Sulfur and Chlorine Source in Nicaragua. *Environ. Sci. Technol.* **2001**, *35*, 1289–1293. [[CrossRef](#)] [[PubMed](#)]
28. Stewart, M.A.; Spivack, A.J. The Stable-Chlorine Isotope Compositions of Natural and Anthropogenic Materials. *Rev. Miner. Geochem.* **2004**, *55*, 231–254. [[CrossRef](#)]
29. Wang, H.; Zhuang, Y.; Wang, Y.; Sun, Y.; Yuan, H.; Zhuang, G.; Hao, Z. Long-term monitoring and source apportionment of PM_{2.5}/PM₁₀ in Beijing, China. *J. Environ. Sci.* **2008**, *20*, 1323–1327. [[CrossRef](#)]
30. Galon-Negru, A.G.; Olariu, R.I.; Arsene, C. Chemical characteristics of size-resolved atmospheric aerosols in Iasi, north-eastern Romania: Nitrogen-containing inorganic compounds control aerosol chemistry in the area. *Atmos. Chem. Phys.* **2018**, *18*, 5879–5904. [[CrossRef](#)]
31. Arsene, C.; Olariu, R.I.; Zarmas, P.; Kanakidou, M.; Mihalopoulos, N. Ion composition of coarse and fine particles in Iasi, north-eastern Romania: Implications for aerosols chemistry in the area. *Atmos. Environ.* **2011**, *45*, 906–916. [[CrossRef](#)]
32. Yokelson, R.J.; Burling, I.R.; Urbanski, S.P.; Atlas, E.L.; Adachi, K.; Buseck, P.R.; Wiedinmyer, C.; Akagi, S.K.; Toohey, D.W.; Wold, C.E.; et al. Trace gas and particle emissions from open biomass burning in Mexico. *Atmos. Chem. Phys.* **2011**, *11*, 6787–6808. [[CrossRef](#)]
33. Cheng, Y.; Engling, G.; He, K.-B.; Duan, F.-K.; Ma, Y.-L.; Du, Z.-Y.; Liu, J.-M.; Zheng, M.; Weber, R.J. Biomass burning contribution to Beijing aerosol. *Atmos. Chem. Phys.* **2013**, *13*, 7765–7781. [[CrossRef](#)]
34. Zhang, J.; Cheng, M.; Ji, D.; Liu, Z.; Hu, B.; Sun, Y.; Wang, Y. Characterization of submicron particles during biomass burning and coal combustion periods in Beijing, China. *Sci. Total Environ.* **2016**, *562*, 812–821. [[CrossRef](#)] [[PubMed](#)]
35. Sun, Y.; Jiang, Q.; Xu, Y.; Ma, Y.; Zhang, Y.; Liu, X.; Li, W.; Wang, F. Aerosol characterization over the North China Plain: Haze life cycle and biomass burning impacts in summer. *J. Geophys. Res. Atmos.* **2016**, *121*, 2508–2521. [[CrossRef](#)]
36. Duce, R.A.; Laroche, J.; Altieri, K.; Arrigo, K.R.; Baker, A.R.; Capone, D.G.; Cornell, S.; Dentener, F.; Galloway, J.; Ganeshram, R.S.; et al. Impacts of Atmospheric Anthropogenic Nitrogen on the Open Ocean. *Science* **2008**, *320*, 893–897. [[CrossRef](#)] [[PubMed](#)]
37. Kim, T.-W.; Lee, K.; Najjar, R.G.; Jeong, H.-D.; Jeong, H.J. Increasing N Abundance in the Northwestern Pacific Ocean Due to Atmospheric Nitrogen Deposition. *Science* **2011**, *334*, 505–509. [[CrossRef](#)] [[PubMed](#)]

38. Liu, X.; Zhang, Y.; Han, W.; Tang, A.; Shen, J.; Cui, Z.; Vitousek, P.; Erisman, J.W.; Goulding, K.; Christie, P.; et al. Enhanced nitrogen deposition over China. *Nature* **2013**, *494*, 459–462. [[CrossRef](#)] [[PubMed](#)]
39. Elser, J.J.; Andersen, T.; Baron, J.S.; Bergström, A.-K.; Jansson, M.; Kyle, M.; Nydick, K.R.; Steger, L.; Hessen, D.O. Shifts in Lake N:P Stoichiometry and Nutrient Limitation Driven by Atmospheric Nitrogen Deposition. *Science* **2009**, *326*, 835–837. [[CrossRef](#)] [[PubMed](#)]
40. Lovett, G.M.; Likens, G.E.; Buso, D.C.; Driscoll, C.T.; Bailey, S.W. The biogeochemistry of chlorine at Hubbard brook, New Hampshire, USA. *Biogeochemistry* **2005**, *72*, 191–232. [[CrossRef](#)]
41. Alcalá, F.J.; Custodio, E.; Alcalá, F. Atmospheric chloride deposition in continental Spain. *Hydrol. Process.* **2008**, *22*, 3636–3650. [[CrossRef](#)]
42. Orehova, T.; Vasileva, T. Evaluation of the atmospheric chloride deposition in the Danube hydrological zone of Bulgaria. *Environ. Earth Sci.* **2014**, *72*, 1143–1154. [[CrossRef](#)]
43. Davies, P.; Crosbie, R. Mapping the spatial distribution of chloride deposition across Australia. *J. Hydrol.* **2018**, *561*, 76–88. [[CrossRef](#)]
44. Kubzova, M.; Krivy, V.; Kreislova, K. Influence of Chloride Deposition on Corrosion Products. *Procedia Eng.* **2017**, *192*, 504–509. [[CrossRef](#)]
45. De la Fuente, D.; Díaz, I.; Alcántara, J.; Chico, B.; Simancas, J.; Llorente, I.; García-Delgado, A.; Jiménez, J.A.; Adeva, P.; Morcillo, M. Corrosion mechanisms of mild steel in chloride-rich atmospheres. *Mater. Corros.* **2016**, *67*, 227–238. [[CrossRef](#)]
46. Ma, Y.; Li, Y.; Wang, F. Corrosion of low carbon steel in atmospheric environments of different chloride content. *Corros. Sci.* **2009**, *51*, 997–1006. [[CrossRef](#)]
47. Dong, J.; Han, E.; Ke, W. Introduction to atmospheric corrosion research in China. *Sci. Technol. Adv. Mater.* **2007**, *8*, 559–565. [[CrossRef](#)]
48. Hsu, S.-C.; Gong, G.-C.; Shiah, F.-K.; Hung, C.-C.; Kao, S.-J.; Zhang, R.; Chen, W.-N.; Chen, C.-C.; Chou, C.C.-K.; Lin, Y.-C.; et al. Sources, solubility, and acid processing of aerosol iron and phosphorous over the South China Sea: East Asian dust and pollution outflows vs. Southeast Asian biomass burning. *Atmos. Chem. Phys. Discuss.* **2014**, *14*, 21433–21472. [[CrossRef](#)]
49. Norris, G.; Duvall, R. *Positive Matrix Factorization (PMF) 5.0 Fundamentals & User Guide*; U.S. Environmental Protection Agency: Washington, DC, USA, 2014.
50. Zhou, L.; Kim, E.; Hopke, P.K.; Stanier, C.; Pandis, S. Mining airborne particulate size distribution data by positive matrix factorization. *J. Geophys. Res. Space Phys.* **2005**, *110*. [[CrossRef](#)]
51. Zhang, Y.; Sheesley, R.J.; Schauer, J.J.; Lewandowski, M.; Jaoui, M.; Offenberg, J.H.; Kleindienst, T.E.; Edney, E.O. Source apportionment of primary and secondary organic aerosols using positive matrix factorization (PMF) of molecular markers. *Atmos. Environ.* **2009**, *43*, 5567–5574. [[CrossRef](#)]
52. Yang, Y.; Zhou, R.; Wu, J.; Yu, Y.; Ma, Z.; Zhang, L.; Di, Y. Seasonal variations and size distributions of water-soluble ions in atmospheric aerosols in Beijing, 2012. *J. Environ. Sci.* **2015**, *34*, 197–205. [[CrossRef](#)]
53. Cao, J.-J.; Shen, Z.-X.; Chow, J.C.; Watson, J.G.; Lee, S.-C.; Tie, X.-X.; Ho, K.-F.; Wang, G.-H.; Han, Y.-M. Winter and summer PM_{2.5} chemical compositions in fourteen Chinese cities. *J. Air Waste Manag. Assoc.* **2012**, *62*, 1214–1226. [[CrossRef](#)]
54. Huang, R.-J.; Zhang, Y.; Bozzetti, C.; Ho, K.-F.; Cao, J.-J.; Han, Y.; Daellenbach, K.R.; Slowik, J.G.; Platt, S.M.; Canonaco, F.; et al. High secondary aerosol contribution to particulate pollution during haze events in China. *Nature* **2014**, *514*, 218–222. [[CrossRef](#)]
55. Ji, D.; Li, L.; Wang, Y.; Zhang, J.; Cheng, M.; Sun, Y.; Liu, Z.; Wang, L.; Tang, G.; Hu, B.; et al. The heaviest particulate air-pollution episodes occurred in northern China in January, 2013: Insights gained from observation. *Atmos. Environ.* **2014**, *92*, 546–556. [[CrossRef](#)]
56. Vieira-Filho, M.; Pedrotti, J.J.; Fornaro, A. Water-soluble ions species of size-resolved aerosols: Implications for the atmospheric acidity in São Paulo megacity, Brazil. *Atmos. Res.* **2016**, *181*, 281–287. [[CrossRef](#)]
57. Liu, Y.; Fan, Q.; Chen, X.; Zhao, J.; Ling, Z.; Hong, Y.; Li, W.; Chen, X.; Wang, M.; Wei, X. Modeling the impact of chlorine emissions from coal combustion and prescribed waste incineration on tropospheric ozone formation in China. *Atmos. Chem. Phys.* **2018**, *18*, 2709–2724. [[CrossRef](#)]
58. Yang, X.; Wang, T.; Xia, M.; Gao, X.; Li, Q.; Zhang, N.; Gao, Y.; Lee, S.; Wang, X.; Xue, L.; et al. Abundance and origin of fine particulate chloride in continental China. *Sci. Total Environ.* **2018**, *624*, 1041–1051. [[CrossRef](#)] [[PubMed](#)]

59. Li, J.; Wang, G.; Zhou, B.; Cheng, C.; Cao, J.; Shen, Z.; An, Z. Chemical composition and size distribution of wintertime aerosols in the atmosphere of Mt. Hua in central China. *Atmos. Environ.* **2011**, *45*, 1251–1258. [[CrossRef](#)]
60. Zhang, N.; Cao, J.; Ho, K.; He, Y. Chemical characterization of aerosol collected at Mt. Yulong in wintertime on the southeastern Tibetan Plateau. *Atmos. Res.* **2012**, *107*, 76–85. [[CrossRef](#)]
61. Zhao, Y.-N.; Wang, Y.-S.; Wen, T.-X.; Yang, Y.-J.; Li, W. Observation and analysis on water-soluble inorganic chemical compositions of atmospheric aerosol in Gongga Mountain. *Huan Jing Ke Xue* **2009**, *30*, 9–13.
62. Zhao, Y.-N.; Wang, Y.-S.; Wen, T.-X.; Dai, G.-H. Seasonal variation of water-soluble ions in PM_{2.5} at Changbai Mountain. *Huan Jing Ke Xue* **2014**, *35*, 9–14.
63. Yang, D.; Yu, X.; Fang, X.; Wu, F.; Li, X. A study of aerosol at regional background stations and baseline station. *Q. J. Appl. Meteorol.* **1996**, *7*, 396–405.
64. Hsu, S.C.; Liu, S.C.; Huang, Y.T.; Chou, C.C.K.; Lung, S.C.C.; Liu, T.H.; Tu, J.Y.; Tsai, F. Long-range southeastward transport of asian biosmoke pollution: Signature detected by aerosol potassium in northern taiwan-article no. d14301. *J. Geophys. Res. Atmos.* **2019**, *114*. [[CrossRef](#)]
65. Weber, R.J.; Lee, Y.; Orsini, D.A.; Maxwell-Meier, K.; Thornton, D.C.; Bandy, A.R.; Clarke, A.D.; Sachse, G.W.; Fuelberg, H.E.; Kiley, C.M.; et al. Characteristics and influence of biosmoke on the fine-particle ionic composition measured in Asian outflow during the Transport and Chemical Evolution Over the Pacific (TRACE-P) experiment. *J. Geophys. Res. Space Phys.* **2003**, *108*, 8816. [[CrossRef](#)]
66. Waldman, J.; Liou, P.; Zelenka, M.; Jing, L.; Lin, Y.; He, Q.; Qian, Z.; Chapman, R.; Wilson, W. Wintertime measurements of aerosol acidity and trace elements in Wuhan, a city in central China. *Atmos. Environ. Part B Urban Atmos.* **1991**, *25*, 113–120. [[CrossRef](#)]
67. Xu, Y.; Liu, X.; Zhang, P.; Guo, J.; Han, J.; Zhou, Z.; Xu, M. Role of chlorine in ultrafine particulate matter formation during the combustion of a blend of high-Cl coal and low-Cl coal. *Fuel* **2016**, *184*, 185–191. [[CrossRef](#)]
68. Yan, Q.; Kong, S.; Liu, H.; Wang, W.; Wu, J.; Zheng, M.; Zheng, S.; Yang, G.; Wu, F. Emission inventory of water soluble ions in fine particles from residential coal burning in China and implication for emission reduction. *China Environ. Sci.* **2017**, *37*, 3708–3721. (In Chinese)
69. Chester, R. *Marine Geochemistry*; Cambridge University Press: London, UK, 1990.
70. Shen, Z.; Sun, J.; Cao, J.; Zhang, L.; Zhang, Q.; Lei, Y.; Gao, J.; Huang, R.-J.; Liu, S.; Huang, Y.; et al. Chemical profiles of urban fugitive dust PM 2.5 samples in Northern Chinese cities. *Sci. Total Environ.* **2016**, *569*, 619–626. [[CrossRef](#)] [[PubMed](#)]
71. Chantara, S.; Thepnuan, D.; Wiriya, W.; Prawan, S.; Tsai, Y.I. Emissions of pollutant gases, fine particulate matters and their significant tracers from biomass burning in an open-system combustion chamber. *Chemosphere* **2019**, *224*, 407–416. [[CrossRef](#)] [[PubMed](#)]
72. Sun, J.; Shen, Z.; Zhang, Y.; Zhang, Q.; Lei, Y.; Huang, Y.; Niu, X.; Xu, H.; Cao, J.; Ho, S.S.H.; et al. Characterization of PM_{2.5} source profiles from typical biomass burning of maize straw, wheat straw, wood branch, and their processed products (briquette and charcoal) in China. *Atmos. Environ.* **2019**, *205*, 36–45. [[CrossRef](#)]
73. Cao, G.; Zhang, X.; Gong, S.; Zheng, F. Investigation on emission factors of particulate matter and gaseous pollutants from crop residue burning. *J. Environ. Sci.* **2008**, *20*, 50–55. [[CrossRef](#)]
74. Guo, F.; Ju, Y.; Wang, G.; Alvarado, E.C.; Yang, X.; Ma, Y.; Liu, A. Inorganic chemical composition of PM_{2.5} emissions from the combustion of six main tree species in subtropical China. *Atmos. Environ.* **2018**, *189*, 107–115. [[CrossRef](#)]
75. Dai, Q.; Bi, X.; Song, W.; Li, T.; Liu, B.; Ding, J.; Xu, J.; Song, C.; Yang, N.; Schulze, B.C.; et al. Residential coal combustion as a source of primary sulfate in Xi'an, China. *Atmos. Environ.* **2019**, *196*, 66–76. [[CrossRef](#)]
76. Shang, Y. Research on Layer Burning Industrial Boiler PM_{2.5} Emissions Characteristics. Master's Thesis, Harbin Institute of Technology, Harbin, 2012. (In Chinese).
77. Xu, J.; Huang, C.; Li, L.; Chen, Y.; Lou, S.; Qiao, L.; Wang, H. Chemical Composition Characteristics of PM_{2.5} Emitted by Medium and Small Capacity Coal-fired Boilers in the Yangtze River Delta Region. *Environ. Sci.* **2018**, *39*, 1493–1501.
78. Huang, W.; Bi, X.; Zhang, G.; Huang, B.; Lin, Q.; Wang, X.; Sheng, G.; Fu, J. The chemical composition and stable carbon isotope characteristics of particulate matter from the residential honeycomb coal briquettes combustion. *Geochimica* **2014**, *43*, 640–646.

79. Oris, C.; Luo, Z.; Zhang, W.; Yu, C. Forms of potassium and chlorine from oxy-fuel co-combustion of lignite coal and corn stover. *Carbon Resour. Convers.* **2019**, *2*, 103–110. [[CrossRef](#)]
80. Zhao, J.; Zhang, F.; Xu, Y.; Chen, J. Characterization of water-soluble inorganic ions in size-segregated aerosols in coastal city, Xiamen. *Atmos. Res.* **2011**, *99*, 546–562. [[CrossRef](#)]
81. Zhang, J.; Tong, L.; Huang, Z.; Zhang, H.; He, M.; Dai, X.; Zheng, J.; Xiao, H. Seasonal variation and size distributions of water-soluble inorganic ions and carbonaceous aerosols at a coastal site in Ningbo, China. *Sci. Total Environ.* **2018**, *639*, 793–803. [[CrossRef](#)] [[PubMed](#)]
82. Li, X.; Wang, L.; Ji, D.; Wen, T.; Pan, Y.; Sun, Y.; Wang, Y. Characterization of the size-segregated water-soluble inorganic ions in the Jing-Jin-Ji urban agglomeration: Spatial/temporal variability, size distribution and sources. *Atmos. Environ.* **2013**, *77*, 250–259. [[CrossRef](#)]
83. Wang, H.; Zhu, B.; Shen, L.; Xu, H.; An, J.; Xue, G.; Cao, J. Water-soluble ions in atmospheric aerosols measured in five sites in the Yangtze River Delta, China: Size-fractionated, seasonal variations and sources. *Atmos. Environ.* **2015**, *123*, 370–379. [[CrossRef](#)]
84. Liu, Z.; Xie, Y.; Hu, B.; Wen, T.; Xin, J.; Li, X.; Wang, Y. Size-resolved aerosol water-soluble ions during the summer and winter seasons in Beijing: Formation mechanisms of secondary inorganic aerosols. *Chemosphere* **2017**, *183*, 119–131. [[CrossRef](#)]
85. Huang, X.; Liu, Z.; Zhang, J.; Wen, T.; Ji, D.; Wang, Y. Seasonal variation and secondary formation of size-segregated aerosol water-soluble inorganic ions during pollution episodes in Beijing. *Atmos. Res.* **2016**, *168*, 70–79. [[CrossRef](#)]
86. Yang, Y.; Zhou, R.; Yan, Y.; Yu, Y.; Liu, J.; Di, Y.; Du, Z.; Wu, D. Seasonal variations and size distributions of water-soluble ions of atmospheric particulate matter at Shigatse, Tibetan Plateau. *Chemosphere* **2016**, *145*, 560–567. [[CrossRef](#)]
87. Li, X.; Wang, L.; Wang, Y.; Wen, T.; Yang, Y.; Zhao, Y.; Wang, Y. Chemical composition and size distribution of airborne particulate matters in Beijing during the 2008 Olympics. *Atmos. Environ.* **2012**, *50*, 278–286. [[CrossRef](#)]
88. Hsu, S.-C.; Liu, S.-C.; Kao, S.-J.; Jeng, W.-L.; Huang, Y.-T.; Tseng, C.-M.; Tsai, F.; Tu, J.-Y.; Yang, Y. Water-soluble species in the marine aerosol from the northern South China Sea: High chloride depletion related to air pollution. *J. Geophys. Res. Space Phys.* **2007**, *112*. [[CrossRef](#)]
89. Wang, G.H.; Huang, Y.; Tao, J.; Ren, Y.Q.; Wu, F.; Cheng, C.L.; Meng, J.J.; Li, J.J.; Cheng, Y.T.; Cao, J.J.; et al. Evolution of aerosol chemistry in Xi'an, inland China during the dust storm period of 2013—Part 1: Sources, chemical forms and formation mechanisms of nitrate and sulfate. *Atmos. Chem. Phys.* **2014**, *14*, 11571–11585. [[CrossRef](#)]
90. Saleh, S.B.; Flensburg, J.P.; Shoulaifar, T.K.; Sárossy, Z.; Hansen, B.B.; Egsgaard, H.; DeMartini, N.; Jensen, P.A.; Glarborg, P.; Dam-Johansen, K. Release of Chlorine and Sulfur during Biomass Torrefaction and Pyrolysis. *Energy Fuels* **2014**, *28*, 3738–3746. [[CrossRef](#)]
91. Dayton, D.C.; Belle-Oudry, D.; Nordin, A. Effect of Coal Minerals on Chlorine and Alkali Metals Released during Biomass/Coal Cofiring. *Energy Fuels* **1999**, *13*, 1203–1211. [[CrossRef](#)]
92. Xiong, H.H.; Liang, L.W.; Zeng, Z.; Wang, Z.B. Dynamic analysis of PM_{2.5} spatial-temporal characteristics in China. *Resour. Sci.* **2017**, *39*, 136–146. [[CrossRef](#)]
93. Guo, H.; Liu, J.; Froyd, K.D.; Roberts, J.M.; Veres, P.R.; Hayes, P.L.; Jimenez, J.L.; Nenes, A.; Weber, R.J. Fine particle pH and gas-particle phase partitioning of inorganic species in Pasadena, California, during the 2010 CalNex campaign. *Atmos. Chem. Phys.* **2017**, *17*, 5703–5719. [[CrossRef](#)]

